
Unsupervisedly Training GANs for Segmenting Digital Pathology with Automatically Generated Annotations

Michael Gadermayr

Institute of Imaging and Computer Vision, RWTH Aachen University
michael.gadermayr at lfb.rwth-aachen.de

Laxmi Gupta

Institute of Imaging and Computer Vision, RWTH Aachen University

Barbara M. Klinkhammer

Institute of Pathology, University Hospital Aachen, RWTH Aachen University

Peter Boor

Institute of Pathology, University Hospital Aachen, RWTH Aachen University

Dorit Merhof

Institute of Imaging and Computer Vision, RWTH Aachen University

Abstract

Recently, generative adversarial networks exhibited excellent performances in semi-supervised image analysis scenarios. In this paper, we go even further by proposing a fully unsupervised approach for segmentation applications with prior knowledge of the objects' shapes. We propose and investigate different strategies to generate simulated label data and perform image-to-image translation between the image and the label domain using an adversarial model. Specifically, we assess the impact of the annotation model's accuracy as well as the effect of simulating additional low-level image features. For experimental evaluation, we consider the segmentation of the glomeruli, an application scenario from renal pathology. Experiments provide proof of concept and also confirm that the strategy for creating the simulated label data is of particular relevance considering the stability of GAN trainings.

1 Motivation

Due to the progressing dissemination of whole slide scanners generating large amounts of digital histological image data, image analysis in this field has recently gained significant importance. Considered applications mostly consist of either segmentation [1, 2], classification [3, 4, 5, 6] or regression tasks [7]. For segmentation tasks, recently fully-convolutional networks [1, 8] yielded excellent performances in combination with a high computational efficiency compared to sliding-window classification. A major challenge in the field of digital pathology is given by a large set of different application scenarios as well as changing underlying data distributions which is due to inter-subject variability, different staining protocols and/or pathological modifications [9]. Each individual application scenario therefore demands large amounts of annotated training data covering

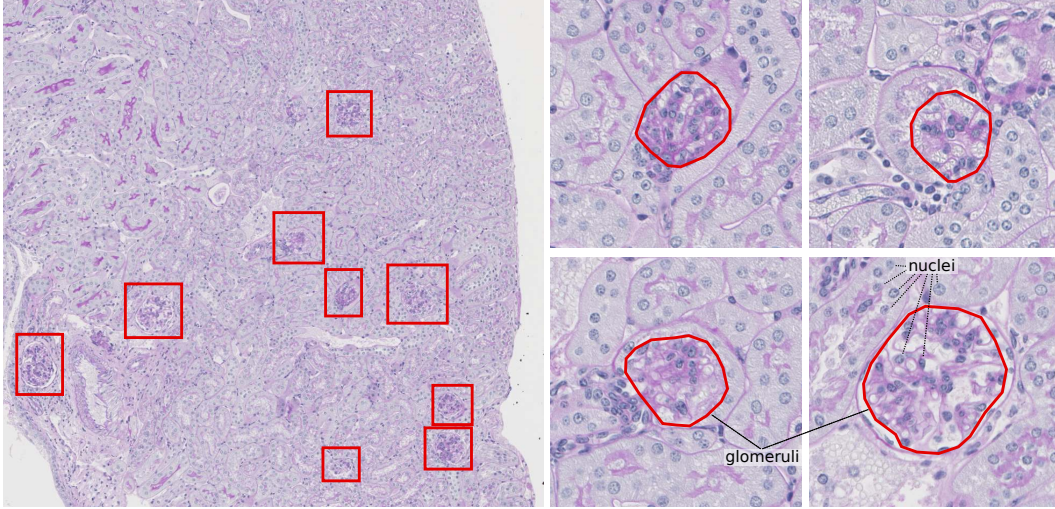


Figure 1: This illustration shows an extract of a renal whole slide image with marked glomeruli (left) as well as magnifications of single glomeruli showing precise manual annotations (right).

the prevalent variability. The acquisition of a large amount of annotated training data (covering all potential image characteristics) is typically time-consuming and cost-intensive and thereby constitutes a major burden for the development and deployment of automated segmentation techniques.

Recently, large effort was taken to train models with a small amount of training data [10]. For training state-of-the-art machine learning approaches such as fully-convolutional networks, especially data augmentation proved to be a highly powerful tool [8, 11]. A limitation of basic as well as advanced, domain specific data augmentation in combination with supervised learning approaches is given by the fact that often large non-annotated data is available "for free" but is not utilized for training at all. Particularly in the fields of medicine, such as digital pathology, huge amounts of digital image data are routinely captured without any (additional) effort whereby a complete annotation of all data is definitely not feasible. In order to take advantage of non-annotated data as well, dedicated semi-supervised segmentation approaches relying on adversarial models were recently proposed [12, 13, 14].

Adversarial models were also developed for the field of image-to-image translation [15, 16]. Recently, the so-called cycleGAN [16] was introduced which eliminates the restriction of corresponding image pairs for training the artificial neural network. The authors proposed a generative adversarial network (GAN) relying on a cycle-consistency loss which is combined with an adversarial loss to perform circular trainings, i.e. translations from a domain X to a domain Y and back to domain X and the same vice versa are conducted. This GAN architecture not only exhibits excellent performance in image-to-image translation applications. It is also utilized for means of unsupervised domain adaptation. For example, images can be converted between MRI and CT in order to finally process (e.g. segment or classify) the images in a (fake) target domain [17, 18]. The huge benefit of this approach is, that it does not require corresponding pairs from both domains which are mostly unavailable or at least difficult to obtain. Additionally, the domain transfer on image-level is completely transparent as an observable fake image is generated.

Contribution: In this work, we tackle the problem of acquiring labeled training data by proposing a framework completely bypassing the need for manually annotating objects. We focus on generating artificial annotations and perform image-to-image translation based on unpaired data between the image and the label domain. In our experimental study, we investigate strategies for modeling the shape of the annotations as well as for modeling additional image information to provide support for training the translation networks. As application scenario, we consider a segmentation task from digital pathology, specifically the segmentation of the renal glomeruli [2, 19] (Fig. 1). Although generally showing high variability in texture, color and size, the overall shape of the objects remains almost stable which is a crucial criterion for the proposed method. This proof-of-concept provides evidence for the applicability in digital pathology. The evaluation of different settings offers incentive for an investigation with respect to further segmentation tasks in (biomedical) image analysis.

2 Methods

For the proposed method, we make use of an image-to-image translation approach. Specifically, we utilize a generative adversarial network (GAN) which facilitates training with unpaired data [16]. The four subnetworks consisting of two generators and two discriminators are optimized based on an adversarial loss as well as a cycle consistency criterion. This formulation does not require sample pairs, i.e. there is no need to obtain corresponding image samples for the two domains. Instead it is sufficient to collect a set of images, individually for each domain.

If annotations are interpreted as label (e.g. binary) images, this approach can be utilized for segmentation applications as well. But it was shown that approaches taking the pair-relationship into consideration exhibit better results [13, 16]. However, obtaining such pairs in a segmentation scenario typically means that each original image needs to be annotated such that a pair consists of an original and a label image.

For unpaired training [16], however, there is no need to generate annotations corresponding to original images. It allows to perform training with a set of images and a set of annotations as long as the annotations are realistic (i.e. the distribution matches the underlying distribution of real annotations). Therefore, such a setting facilitates training with one data set containing images and one data set containing artificially generated annotations.

The proposed method relies on an automated generation of realistic annotation images followed by training an image-to-image translation model which is finally able to convert original images to annotations. This procedure is based on the following assumptions:

1. We need to understand the underlying distribution of the annotation data and we need to be able to model this distribution (for details, see Sect. 2.1).
2. The unpaired image-to-image translation approach needs to be effectively applicable to translate between the image and the annotation domain. If a straight-forward translation is not effective, additional information can be added to the annotation domain to enhance the translation process (for details, see Sect. 2.2).

2.1 Annotation Model

In the considered application scenario (Fig. 1), the underlying distribution (assumption 1) of the objects-of-interest is rather basic and can thereby be approximately modeled quite well. The objects-of-interest show roundish shapes which are sparsely distributed over the kidney. For training we consider patches extracted from the whole slide images. We assume that the number of objects per patch can be approximated by a (quantized) Gaussian distribution $G_{\#} \sim \mathcal{N}(\mu_g, \sigma_g^2)$. The objects are uniformly distributed over the patch with one single further assumption that the objects may not overlap. For generating the annotations, we investigate two different approaches:

- Circular objects (C): firstly, we consider the objects-of-interest as round objects. The objects' radii r are randomly sampled from a Gaussian distribution $R \sim \mathcal{N}(\mu_r, \sigma_r^2)$.
- Elliptic objects (E): in a second configuration, we incorporate the fact that the objects-of-interest often show an elliptic shape. To incorporate this knowledge, r_1 is drawn from the same distribution as r and $r_2 = r_1 + r_\delta$ where r_δ models the eccentricity and is drawn from $R_\delta \sim \mathcal{N}(0, \sigma_e^2)$. A further rotation parameter α is drawn from a uniform distribution in the interval $[0, 2\pi]$.

2.2 Enhanced Image-to-Image Translation

The straightforward approach consists of adding either circles or ellipses as binary objects into two dimensional matrices which are interpreted as single channel images. However, for training the image-to-image translation approach, this setting can be highly challenging due to the loss criteria:

For training the GAN [16], two generative models, $F : \mathcal{X} \rightarrow \mathcal{Y}$ and $G : \mathcal{Y} \rightarrow \mathcal{X}$ and two discriminators D_X and D_Y are trained optimizing the cycle consistency loss

$$\mathcal{L}_c = \mathbb{E}_{x \sim p_{data}(x)} [\|G(F(x)) - x\|_1] + \mathbb{E}_{y \sim p_{data}(y)} [\|F(G(y)) - y\|_1] \quad (1)$$

as well as the adversarial loss

$$\mathcal{L}_d = \mathbb{E}_{x \sim p_{data}(x)} [\log(D_X(x)) + \log(1 - D_Y(F(x)))] + \mathbb{E}_{y \sim p_{data}(y)} [\log(1 - D_X(G(y))) + \log(D_Y(y))] \quad (2)$$

where F and G try to generate fake images that look similar to real images, while D_X and D_Y aim to distinguish between translated and real samples. The generators aim to minimize this adversarial objective against the discriminators that try to maximize it.

Let X be the domain referring to the original images and let Y be the label domain. The cycle criterion requires that an annotation mask can be translated to an image by the generator G . The generator F , however, hides all low-level image details, such as nuclei and tubuli (Fig. 1) and only preserves the high-level shapes of the glomeruli. Based on these shapes only, it will not be able to reconstruct e.g. the nuclei at the right (i.e. the same) positions leading to a high cycle-consistency loss even though the images might look realistic. To take this into account, we propose and investigate a second setting simulating the nuclei exhibiting low-level information as well. As for the glomeruli, the number of nuclei is drawn from a (quantized) normal distribution $N_{\#} \sim \mathcal{N}(\mu_n, \sigma_n^2)$. They are uniformly distributed over the whole patch with the restriction that they may not overlap. Diameter is fixed to d_n . The additional binary matrix containing the nuclei is added as further image channel to the annotation image. This channel is only needed to train the GAN. For testing, this further channel is simply ignored. Whereas the setting incorporating only the target labels (i.e. the glomeruli) is referred to as single-class scenario, the setting also incorporating further low-level information is referred to as multi-class scenario. Finally, we identified four different settings: single-class circular objects (SC), single-class elliptical objects (SE), multi-class circular objects (MC) and multi-class elliptical objects (ME).

To facilitate learning, Gaussian random noise (σ_{f_n}) is added to the annotation maps followed by the application of a Gaussian filter (σ_{f_s}) to smooth the objects' borders in all settings.

2.3 Image Data

Paraffin sections ($1\mu m$) are stained with periodic acid-Schiff (PAS) reagent and counterstained with hematoxylin. Whole slides are digitalized with a Hamamatsu NanoZoomer 2.0HT digital slide scanner and a $20\times$ objective lens.

From overall 20 WSIs, image patches with a size of 500×500 pixels are extracted. For evaluation purpose, all WSIs are manually annotated under the supervision of a medical expert. From each image, 100 patches are extracted randomly from the cortex of the kidney which contains the glomeruli. The anatomical structure of the organ allows easy manual delineation of this part because it shows a clear change in texture. As large context is required rather than small details to assess whether segmentations are realistic, a resolution corresponding to a $2.5\times$ magnification is utilized, i.e. the highest ($20\times$) resolution images are downsampled by factor 8.

2.4 Experimental Setting

For image-to-image translation, we make use of the cycle GAN as proposed in [16]. We rely on the provided pytorch reference implementation. Apart from the mentioned changes, we use the proposed standard settings. As generator model, a residual network consisting of four blocks is utilized. As discriminator, we rely on the suggested patch-wise CNN with three layers [16]. Learning rate is fixed to 10^{-6} , number of training epochs is set to 15 and batch size is set to one.

In the annotation masks, positive pixels are set to 155 and negative pixels are set to 100 (instead of 255 and 0 corresponding to min and max in the eight bit images) to facilitate the addition of noise in both directions. For training, subimages with a size of 384×384 pixels are randomly selected in each iteration. The cycle consistency loss and the adversarial loss are equally weighted. No further loss (e.g. identity loss) is used.

The annotations are generated based on the following parameters: $\mu_g = 7$, $\sigma_g = 2$, $\mu_r = 18$, $\sigma_r = 2$, $\sigma_e = 2$, $d_n = 4$, $\mu_n = 5000$, $\sigma_n = 50$, $\sigma_{f_n} = 5$ and $\sigma_{f_s} = 2$. These parameters were obtained by visual assessment of a small subset of the image data. We did not quantitatively analyze the ground-truth annotations (which are available for evaluation purpose) in order to avoid introducing a significant amount of supervision and thereby bias to the unsupervised application scenario.

For final evaluation, we investigate two optimization strategies. The first strategy does not incorporate any optimization and we basically report the obtained segmentation performance after training for all 15 epochs. As GAN training is, in general, often unstable, we also optimize the epoch by separating the testing data set into one patch for optimization and the others for testing. We use only one patch for optimization because the approach is intended to be unsupervised while optimization requires annotated patches. Nevertheless, the effort required for annotating one patch only is negligible. We also report the aggregated testing performance individually after each epoch to assess convergence of the GAN.

Apart from pixel-level scores (F_1 -score (F), precision (P), recall(R)), we also report the corresponding object-level scores (F_o , P_o , R_o). That means, we distinguish between true positive objects (i.e. the distance between the center of a detected object and a real object is smaller than 10 pixels), objects which were missed and false positively detected objects.

As we do not make use of real label data during training, training and testing is performed on the same (whole) data set without introducing any bias. To exclude random effects, all experiments are repeated eight times. The obtained performances are compared with the a supervised fully-convolutional network. We utilize a network which was already applied effectively to the considered application scenario. Specifically, we employ a shallow version of the U-net [2, 8] which showed good performances on downscaled WSIs. For details on training and augmentation, we refer to [2]. The experiments are conducted on a NVIDIA GeForce GTX 1080 Ti GPU.

3 Results

Fig. 2 shows quantitative results for each of the four different settings. We investigate pixel-level as well as object-level scores. The left two columns show the testing pixel-level and object-level F_1 -scores for different numbers of training epochs. The third column shows the scores obtained with cross validation (i.e. the epoch is optimized) and the last column shows the rates corresponding to training for 15 epochs without any further optimization.

Considering these results, we notice that the single-class settings (SC, SE) do not show any useful results. In case of elliptical shapes (SE), at least the best configuration exhibits acceptable outcomes, however, GAN training is highly unstable in this scenario. In case of the multi-class settings (MC, ME), we notice a more stable behavior, as in each repetition good scores are obtained after few training epochs. Mean pixel-level F_1 -scores of 0.63 (MC) and 0.62 (ME) as well as mean object-level F -scores of 0.74 (MC and ME) are achieved. Convergence is obtained approximately after six epochs for both settings. We notice slightly higher precision than recall, especially on object-level. A further optimization of the number the training epoch does not show a high influence.

The baseline results of the supervised approach are provided in Fig. 3. We notice that the break-even point of the supervised approach is reached with approximately four fully-annotated training WSIs corresponding to roughly 500 annotated glomeruli. Considering the object-level scenario, the proposed method exhibits even better performances (comparable with the supervised method trained on eight WSIs).

Example output of the image-to-image translation process is provided in Fig. 4. With the single-class setting ((a)–(b)), we notice a tendency to segment vessel structures instead of the target objects. This is not the case if making use of the multi-class settings ((c)–(d)). Qualitative segmentation results obtained with the MC setting are provided in Fig. 5. We notice that especially small objects are often not detected partly leading to weak object-level F_1 -scores. Additionally, we notice that in some cases only a small part of the object is segmented explaining the partially weak pixel-level scores.

4 Discussion

In this work, we investigated a concept of fully-unsupervised learning for segmentation applications by making use of a GAN in combination with simulated annotation data.

We obtained highly divergent results for the four different settings. One substantial finding is that a simulation of the annotations of the objects-of-interest only (referred to as single-class scenario) is not sufficient to obtain proper segmentations of the glomeruli in the investigated unpaired image-to-image translation scenario. In the majority of attempts, an unwanted translation between the image and

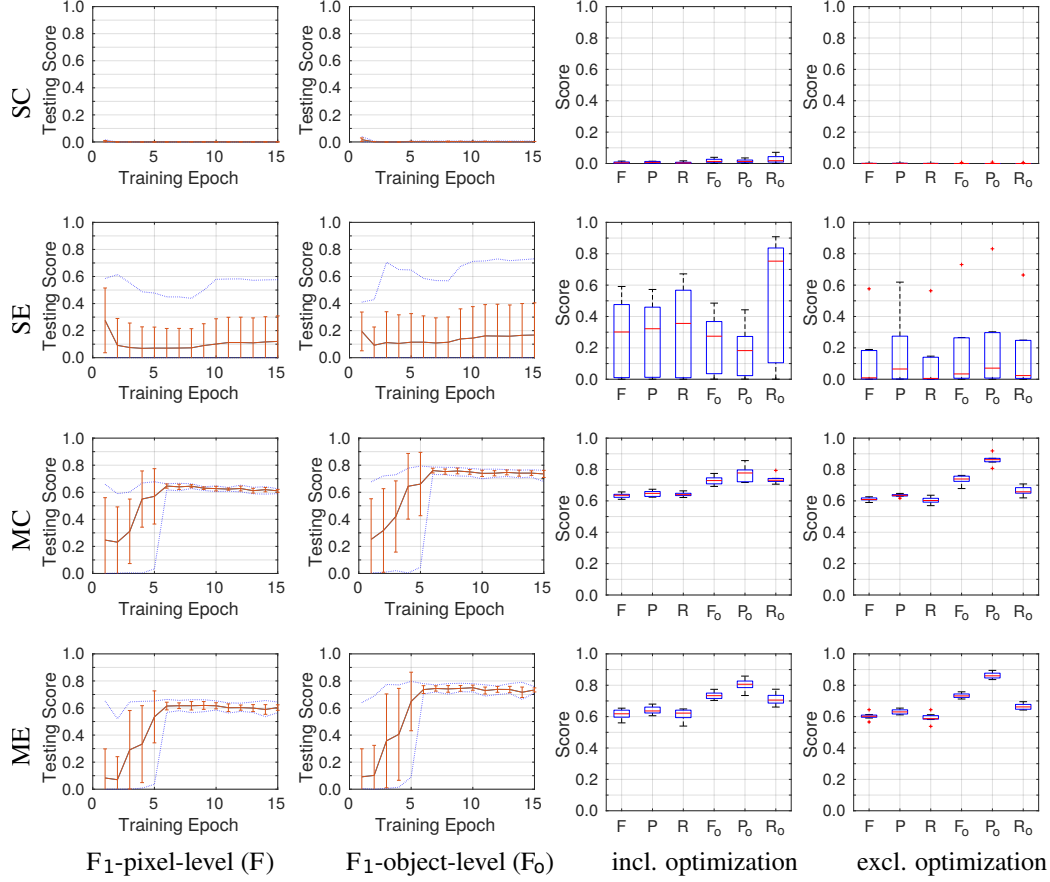


Figure 2: Experimental results for the four different settings (row 1 to row 4). The left columns show pixel- and object-level F₁-scores for testing after varying number of training epochs. The right columns provide F₁-scores (F), precision (P) and recall (R) as well as object-level measures (F_o, P_o, R_o) for training for 15 epochs (excl. optimization) and for optimizing the epoch (incl. optimization).

the label domain is observed. A major problem here is that a translation from the label to the image domain cannot be performed which complicates the GAN training. The generator G in this case has no chance to place the low-level objects (here the nuclei) in a way that the cycle consistency loss can become small as the position of the nuclei cannot be effectively derived from the annotation image. This behavior can also be seen in the example reconstructed images where nuclei cannot be clearly detected (Fig. 4, third column).

In the multi-class scenarios with added simulated nuclei during GAN training, these objects are maintained during the training cycles. That means, the nuclei are segmented during translation to the label domain followed by a reconstruction of the nuclei based on the label domain in case of the inverse mapping. Interestingly, the texture of the glomeruli is still not reconstructed appropriately, which is likely due to the fact that the nuclei inside the glomeruli exhibit different properties (they are smaller and more elliptic) and are not perfectly segmented. However, this obviously does not strongly influence the final segmentation performance. Due to the small overall area of the glomeruli, the reconstruction error does not strongly influence the network's overall effectiveness.

A further interesting finding is that the distribution of the shapes of the simulated objects does not have a major impact on final segmentation performance. We do not consider the single-class scenarios here as they showed either completely wrong or highly unstable performance. The multi-class scenarios show similar performances for the setting based on circles and for the setting based on ellipses. Considering the multi-class settings MC and ME, we assess the obtained segmentation performance as good and applicable in medical research and practice although the scores seem to be rather low. We need to mention here that this is on the one hand due to the fact that small objects are often not

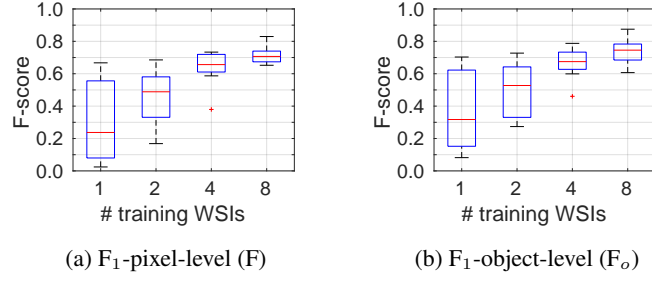


Figure 3: Baseline pixel-level (a) and object-level (b) F_1 -scores indicating the segmentation performance of the supervised U-net-based approach [2] with variable numbers of fully-annotated training WSIs. One single training WSI contains on average 120 single objects.

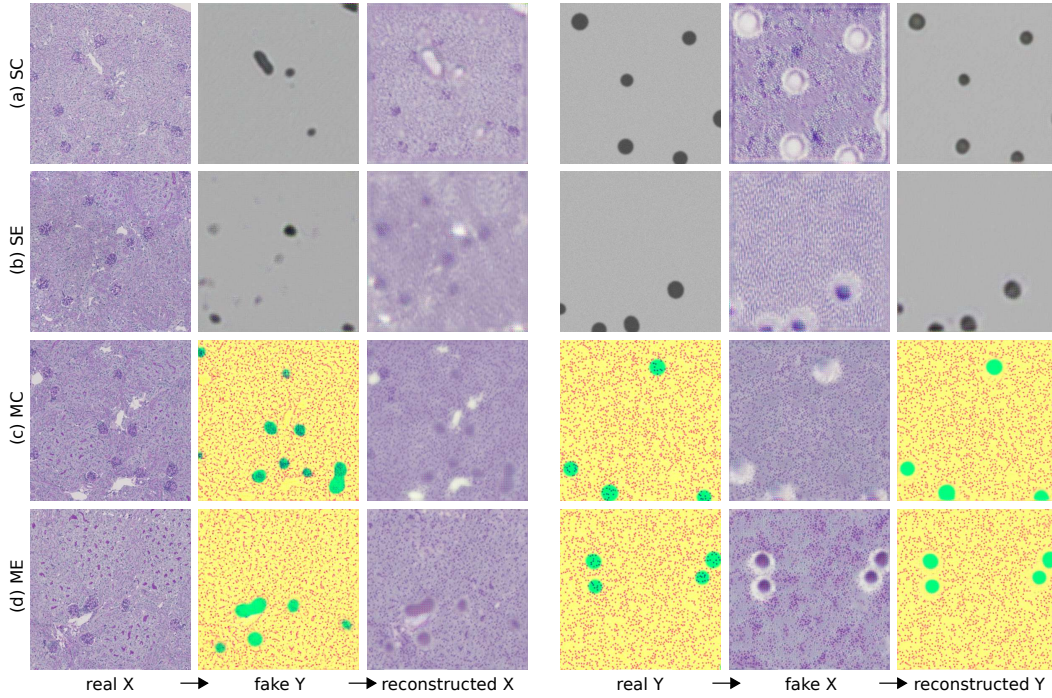


Figure 4: Qualitative results of the image translation process for the four different settings (a) – (d): the finally relevant translation from real X (image domain) to fake Y (annotation domain) is shown on the left side. The other translations are shown to visually assess the cycle consistency criterion.

identified as glomeruli in the ground-truth but are detected by our approach. On the other hand, there are also small objects which are in the ground-truth but are not detected. Anyway, these objects are neglected by the medical experts and are thereby excluded from further analysis. We do not consider a changed evaluation setting, in order to be able to compare the final scores. Often we also notice that only a small part of the objects is segmented (which is also indicated by low pixel-level scores compared to the high object-level scores). In order to improve the pixel-level behavior, a further iterative training approach could be applied as post-processing [20] which could also be combined with higher image resolutions.

For the proposed fully-unsupervised method, we did not consider an application to high resolution data so far, because the discriminator networks need large context in order to appropriately estimate whether an annotation is realistic or not. Therefore, if the image resolution is increased, the network architectures would also need to be changed accordingly. However, also from functional's perspective, a segmentation on the considered resolution is already highly useful.

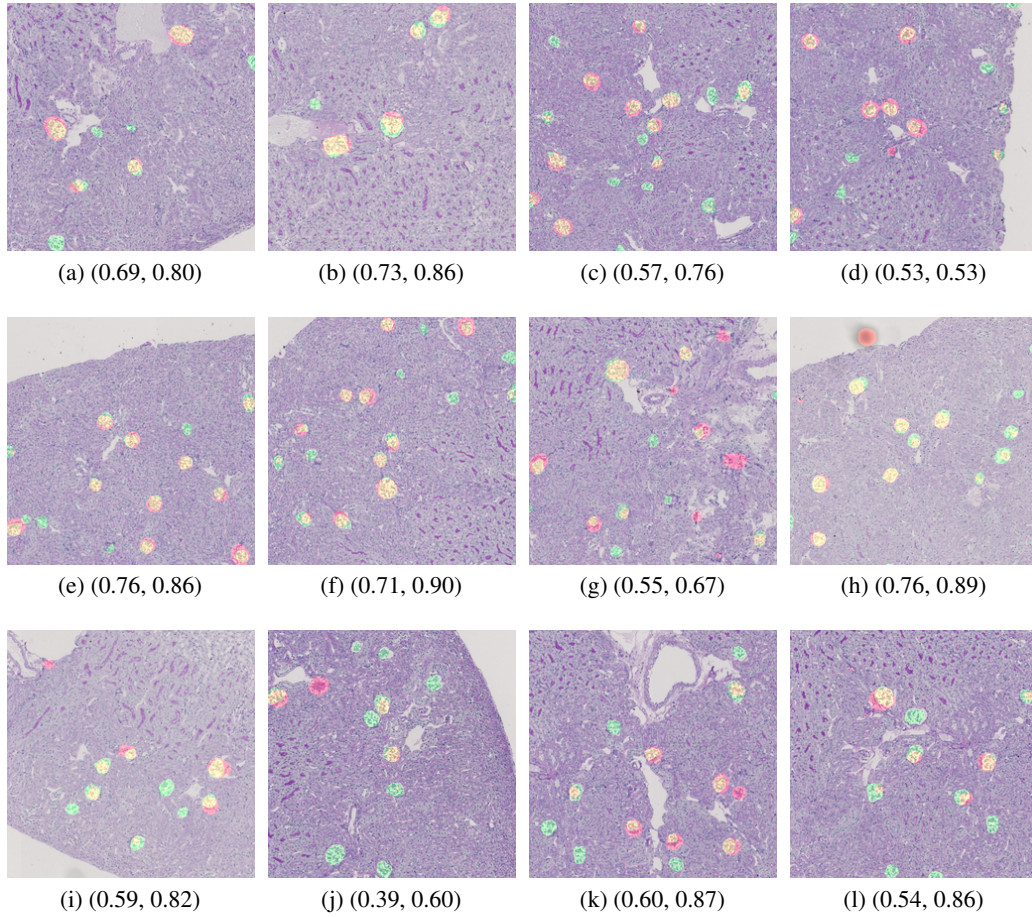


Figure 5: Randomly selected example images including an overlay of the ground-truth annotation (green) and the segmentation output (red) obtained with the MC setting. In the subcaptions, the pixel-level and object-level F_1 -scores are given for each patch (in this order).

A comparison with a state-of-the-art supervised approach showed that the novel method is highly competitive. Especially the detection performance (indicated by the object-level F_1 -scores) is outperformed by the supervised technique only if training is performed with a large amount of annotated data (specifically with eight WSIs corresponding to approx. 1000 single objects). Due to the stable training process, a "slightly-supervised" optimization of the training epoch is not required as the results are only marginally improved (Fig. 2, column 3 vs. column 4).

The most notable advantage, however, does not consist in high scores, but in a very high flexibility. The method can be easily adapted e.g. to other stains without a need for collecting novel annotated training data. Other applications can be handled as well by changing the simulation model. Considering other application scenarios, a requirement is that the annotation data shows regularity and can be modeled effectively. If the objects-of-interest exhibit arbitrary shape, a conversion will not be possible based on unpaired data because a discriminator will not be able to distinguish between real and fake annotations. However, many segmentation tasks in biomedicine show such regular patterns and are thereby ideally suited for being processed with the proposed technique.

5 Conclusion

In this work, we proposed and investigated a concept of fully-unsupervised learning for segmentation applications by making use of a GAN trained with real images and simulated annotations. The experimental results, in general highly promising, indicate that it is not crucial to accurately model

the underlying shape as long as a good approximation is available. This is a highly relevant finding as the shapes of the objects-of-interest are often too complex to be modeled accurately. It is clearly more relevant to support the GAN to fulfill the cycle consistency criterion. Adding additional information to the label domain proved to be an effective way to facilitate the unpaired training process. To apply the proposed strategy to other application scenarios, the challenge consists in modeling the annotations and, even further, to model low-level structure to support the cyclic training process. A comparison with a state-of-the-art supervised segmentation approach shows that the novel method is only outperformed if huge amounts of annotated training data are available.

References

- [1] Aicha BenTaieb and Ghassan Hamarneh. Topology aware fully convolutional networks for histology gland segmentation. In *Proceedings of the International Conference on Medical Image Computing and Computer-Assisted Intervention (MICCAI'16)*, pages 460–468. 2016.
- [2] Michael Gadermayr, Ann-Kathrin Dombrowski, Barbara Mara Klinkhammer, Peter Boor, and Dorit Merhof. CNN cascades for segmenting whole slide images of the kidney. *CoRR*, <https://arxiv.org/abs/1708.00251>, 2017.
- [3] Le Hou, Dimitris Samaras, Tahsin M. Kurc, Yi Gao, James E. Davis, and Joel H. Saltz. Patch-based convolutional neural network for whole slide tissue image classification. In *Proceedings of the International Conference on Computer Vision (CVPR'16)*, 2016.
- [4] Jocelyn Barker, Assaf Hoogi, Adrien Depeursinge, and Daniel L. Rubin. Automated classification of brain tumor type in whole-slide digital pathology images using local representative tiles. *Medical Image Analysis*, 30:60–71, 2016.
- [5] Olcay Sertel, Jun Kong, Hiroyuki Shimada, Umit V. Catalyurek, Joel H. Saltz, and Metin N. Gurcan. Computer-aided prognosis of neuroblastoma on whole-slide images: Classification of stromal development. *Pattern Recognition*, 42(6):1093–1103, jun 2009.
- [6] Mira Valkonen, Kimmo Kartasalo, Kaisa Liimatainen, Matti Nykter, Leena Latonen, and Pekka Ruusuvaori. Dual structured convolutional neural network with feature augmentation for quantitative characterization of tissue histology. In *Proceedings of the IEEE International Conference on Computer Vision (ICCV'17)*, 2017.
- [7] Mitko Veta, Paul J. van Diest, and Josien P. W. Pluim. Cutting out the middleman: Measuring nuclear area in histopathology slides without segmentation. In *Proceedings of the International Conference on Medical Image Computing and Computer-Assisted Intervention (MICCAI'16)*, pages 632–639. 2016.
- [8] Olaf Ronneberger, Philipp Fischer, and Thomas Brox. U-net: Convolutional networks for biomedical image segmentation. In *Proceedings of the International Conference on Medical Image Computing and Computer Aided Interventions (MICCAI'15)*, pages 234–241. 2015.
- [9] Michael Gadermayr, Dennis Eschweiler, Barbara Mara Klinkhammer, Peter Boor, and Dorit Merhof. Gradual domain adaptation for segmenting whole slide images showing pathological variability. In *International Conference on Image and Signal Processing (ICISP'18)*, Springer LNCS, 2018.
- [10] Michael Gadermayr, Dennis Eschweiler, Abiramjee Jeevanesan, Barbara Mara Klinkhammer, Peter Boor, and Dorit Merhof. Segmenting renal whole slide images virtually without training data. *Computers in Biology and Medicine*, 90:88–97, 2017.
- [11] Alexander J. Ratner, Henry R. Ehrenberg, Zeshan Hussain, Jared Dunnmon, and Christopher Re. Learning to compose domain-specific transformations for data augmentation. In *Proceedings of the Conference on Neural Information Processing Systems (NIPS'17)*, 2017.
- [12] Mateusz Kozłowski, Loïc Simon, and Frédéric Jurie. An Adversarial Regularisation for Semi-Supervised Training of Structured Output Neural Networks. In *Proceedings of the Conference on Neural Information Processing Systems (NIPS'17)*, 2017.
- [13] Phillip Isola, Jun-Yan Zhu, Tinghui Zhou, and Alexei A Efros. Image-to-image translation with conditional adversarial networks. In *Proceedings of the International Conference on Computer Vision and Pattern Recognition (CVPR'17)*, 2017.

- [14] Wei-Chih Hung, Yi-Hsuan Tsai, Yan-Ting Liou, Yen-Yu Lin, and Ming-Hsuan Yang. Adversarial learning for semi-supervised semantic segmentation. *CoRR*, <https://arxiv.org/abs/1802.07934>, 2018.
- [15] Justin Johnson, Alexandre Alahi, and Li Fei-Fei. Perceptual losses for real-time style transfer and super-resolution. In *Proceedings of the European Conference on Computer Vision (ECCV'16)*, 2016.
- [16] Jun-Yan Zhu, Taesung Park, Phillip Isola, and Alexei A Efros. Unpaired image-to-image translation using cycle-consistent adversarial networks. In *Proceedings of the International Conference on Computer Vision (ICCV'17)*, 2017.
- [17] Agisilaos Chartsias, Thomas Joyce, Rohan Dharmakumar, and Sotirios A. Tsaftaris. Adversarial image synthesis for unpaired multi-modal cardiac data. In *Proceedings of the International MICCAI Workshop Simulation and Synthesis in Medical Imaging (SASHIMI'17)*, pages 3–13, 2017.
- [18] Jelmer M. Wolterink, Anna M. Dinkla, Mark H. F. Savenije, Peter R. Seevinck, Cornelis A. T. van den Berg, and Ivana Išgum. Deep MR to CT synthesis using unpaired data. In *Proceedings of the International MICCAI Workshop Simulation and Synthesis in Medical Imaging (SASHIMI'17)*, pages 14–23, 2017.
- [19] Tsuyoshi Kato, Raissa Relator, Hayliang Ngouv, Yoshihiro Hirohashi, Osamu Takaki, Tetsuhiro Kakimoto, and Kinya Okada. Segmental HOG: new descriptor for glomerulus detection in kidney microscopy image. *BMC Bioinformatics*, 16(1), 2015.
- [20] Anna Khoreva, Rodrigo Benenson, Jan Hosang, Matthias Hein, and Bernt Schiele. Simple does it: Weakly supervised instance and semantic segmentation. In *Proceedings of the IEEE Conference on Computer Vision and Pattern Recognition (CVPR'17)*, 2017.